Single-Switch Open-Circuit Diagnosis Method Based on Average Voltage Vector for Three-Level T-Type Inverter

Yiqing Liang, Rongkun Wang, and Bingtao Hu

***Abstract*—Fault-tolerant control strategy plays a significant role in improving the reliability of three-level T-type inverter where fault diagnosis method is the key and a research hotspot. Load power factor variation and modulation index regulation have great effect on conventional load current based diagnosis methods. Therefore, this article proposes a novel voltage vector based method for single-switch open-circuit fault diagnosis in three-level T-type inverter. Average output voltage vector calculated by voltages between dc-link neutral-point and bridge output terminals is taken as the eigenvector in the procedure and failed switch can be located by three diagnosis variables including angle of eigenvector, normalized modulus of eigenvector, and neutral-point potential. These variables will be some certain values under circuit fault, which are defined as eigenvalues. The vector trajectory prediction technology is utilized for threshold setting, by which the diagnosis is suitable for different power factors and different modulation indices. The strategy of redundant vector replacement is applied to realize fault-tolerant operation and verifying the proposed scheme. Simulations and experiments are carried out to illustrate the superiorities of the proposal.**

***Index Terms*—Average voltage vector, fault diagnosis, fault-tolerant operation, single-switch open-circuit fault, three-level T-type inverter.**

I. Introduction

VOLTAGE source inverter is widely used in power systems, aerospace, metallurgy, mining, rail transit, and other fields, where the efficiency and current total harmonic distortion (THD) of the inverter are two important performance indicators in application design. The improvement of output quality can be achieved by increasing switching frequency that also causes more switching loss. These two factors are contradictory and it is necessary to find a compromise proposal. For instance, two-level inverters usually operate at medium switching frequencies (4 to 30 kHz) [1], where both the switching loss and THD could be accepted.

Manuscript received October 24, 2019; revised February 4, 2020 and April 20, 2020; accepted June 2, 2020. Date of publication June 16, 2020; date of current version September 4, 2020. This work was supported in part by the National Natural Science Foundation of China under Grant 51707068 and in part by the Natural Science Foundation of Fujian Province under Grant 2017J01097. Recommended for publication by Associate Editor J. Biela. *(Corresponding author: Rongkun Wang.)*

The authors are with the School of Information Science and Engineering, Huaqiao University, Xiamen 361021, China (e-mail: liangyiqing19@mails.ucas.edu.cn; wangrongkun@hqu.edu.cn; 459282014@qq.com).

Color versions of one or more of the figures in this article are available online at https://ieeexplore.ieee.org.

Digital Object Identifier 10.1109/TPEL.2020.3003058

With the requirement of higher output quality and higher efficiency of inverter, three-level inverter has received more attention by scholars and engineers, where three-level neutral point clamped (3L-NPC) inverter [2]–[4] and three-level T-type inverter ($3LT^2I$) [5], [6] are two popular topologies.

Compared with 3L-NPC inverter, $3LT^2I$ saves two diodes in each bridge with lower rated voltage requirement of two neutral-point connected switches (horizontal switches in $3LT^2I$). Additionally, conduction losses are considerably reduced in $3LT^2I$ because only one switch is flowed through by load current whereas 3L-NPC inverter uses two switches to block the full dc-link voltage, which results in fewer total losses in medium switching frequencies [5], [6].

$3LT^2I$ has advantages of lower rated voltage requirement for switches, higher efficiency, and less harmonic components of output than two-level inverter, which relieves the constraint between efficiency and output quality [7]. Besides, it has twice as many switches as that in two-level inverter and is able to operate under some fault conditions by fault-tolerant control methods [8]–[10]. Therefore, $3LT^2I$ is suitable for applications requiring high output quality and continuity.

Device fault includes short-circuit fault and open-circuit fault, and the former can be converted to the latter by implanting fuses in $3LT^2I$ [11]. Open-circuit diagnosis and fault-tolerant control applications are essential for inverters to improve the stability by avoiding operation with fault switch, which abandons output current distortion, voltage distortion, abnormal load operation, overheating, and etc. Currently, open circuit fault diagnosis methods can be roughly classified into two categories, namely current-based methods and voltage-based methods [12], [13].

Current-based methods save the space and cost of inverters with no requirement of extra sensors that are suitable for applications in narrow space. The load currents are utilized in conventional current-based methods, which has been widely applied in two-level inverter systems [14]–[17]. Phase current-based methods are sensitive to the load regulation and have difficulty finding an appropriate threshold. Hence, they may misdiagnose when load currents change rapidly. Some optimization methods, therefore, have been proposed. For instance, zero-sequence current based method overcomes the load regulation effects [14], and load current principle-component-based method is suitable for conditions with different types of load [15]. Moreover, the eigenvalues of diagnosis variables vary with modulation index, where a dynamic threshold is needed. A method with

normalization is proposed to simplify the calculation, and near-zero zone analysis is applied to improve the reliability of diagnosis [16], [17].

It may have some limitations of current-based methods in three-level inverters because there are more kinds of fault conditions to be distinguished. More information and more complicated algorithm are needed to confirm the fault accurately. Faulty switch can be located by the average normalized current and neutral-point potential in average current methods [18], [19]. In current vector method (CVM), modulus and angle of average current vector are taken as the diagnosis variables to locate the fault [20], where normalization can be utilized to deal with the different amplitudes of load currents. The eigenvalue of normalized modulus in CVM under fault conditions varies with power factor. Typically, when the load currents are capacitive, the eigenvalue decreases greatly and the diagnosis becomes less sensitive to fault conditions. Recently, an on-line diagnosis method monitoring dc-bus neutral-point current and phase currents is investigated for single-switch open-circuit fault [21]. The method is based on the relationship between failed switch and current direction, confirming the diagnosis result in several switching cycles. But it may have some trouble under small current conditions.

Voltage-based methods are less affected by the load current, with the need of additional voltage sensors. Currently, methods based on ac-side voltage are conventional for fault diagnosis, especially in two-level inverters. Load phase voltages could be used for diagnosis in two-level inverters carrying star-connection load [22]. Line-to-line voltage-based method is more preferred as the neutral point of load is difficult to measure in most industrial application [23], [24]. Preprocessing method can extract fault eigenvalues from the theoretical analysis of line-to-line voltage to minimize the influence of load [23]. Fast Fourier transformation and harmonic analysis of line-to-line voltage by Bayesian network can locate the fault switch quickly and accurately [24]. Nevertheless, it is greatly affected by the system parameters and is difficult to get enough samples for training.

It is not easy for voltage-based method to diagnosis in three-level inverters as well. Some switch monitoring methods are proposed to locate the faults responsibly and quickly [25], [26]. An early fault detection by analyzing the insulated gate bipolar transistor (IGBT) gate signal behavior during turn-ON transient has been proposed for one specific switch tube diagnosis [25]. The complex hardware requirement is the biggest limitation of this method in multilevel converter. Another real-time diagnosis of multiple faults for neutral point clamped (NPC) inverter is achieved by logic relationship between the voltages across upper half-bridge switches and corresponding switching signals [26]. Additionally, a diagnosis method is presented for active-NPC utilizing load pole voltages, phase currents, and switching states information [27], which can confirm the fault within one fundamental cycle.

In this article, a single-switch fault diagnosis method, voltage vector method (VVM), is proposed for 3LT^{2}I, which is directly inherited from conventional CVM. Neutral-point potential and average voltage vector in a fundamental cycle calculated by filtered voltages between bridge output terminals and neutral-point are utilized to confirm fault location. Voltage trajectory prediction and normalization are applied to make the method more reliable under different load power factors (PFs) and different modulation indices. It needs to be emphasized that average voltage vector in this article refers particularly to the vector composed by three voltages between dc-link neutral-point and bridge output terminals.

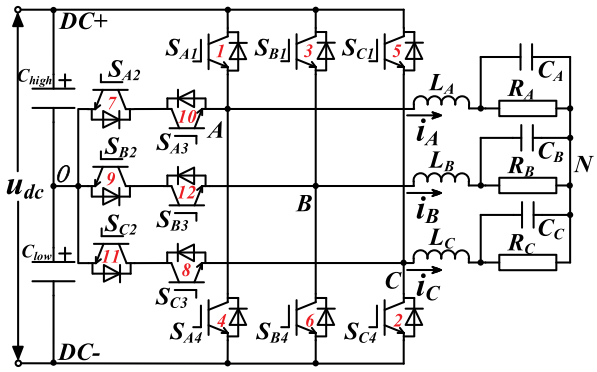

Fig. 1. Schematic of three-level T-type inverter topology.

TABLE I
SWITCH STATE AND OUTPUT POTENTIAL OF EACH BRIDGE OF 3LT^{2}I

Switch State	S_{X1}	S_{X2}	S_{X3}	S_{X4}	u_{XO}
P	1	0	1	0	$u_{dc}/2$
O	0	1	1	0	0
N	0	1	0	1	$-u_{dc}/2$

II. TOPOLOGY OF THREE-LEVEL T-TYPE INVERTER

The circuit topology of 3LT^{2}I is shown as Fig. 1. There are two dc-link capacitors between dc-link buses including a passive node "O" named dc-link neutral point. The neutral-point potential is recognized as zero when the voltages of $C_{\rm high}$ and $C_{\rm low}$ are equal. Small amplitude ripple of the capacitors' voltage can be ignored and three potentials can be obtained including $u_{\rm dc}/2$, 0, and $-u_{\rm dc}/2$ from each bridge. Voltages between neutral point "O" and three bridge output terminals "A", "B", and "C" are named u_{AO}, u_{BO}, and u_{CO}, which are the main parameters in this article. Relationships between switch states and output potentials are shown as Table I, where "$S_{X1}=1$" represents ON state of S_{X1}, and "$S_{X1}=0$" represents OFF state of S_{X1}.

The output voltage vector of 3LT^{2}I can be calculated by state of three bridges as follows:

$$\begin{aligned}\boldsymbol{u}_{inv} &= ku_{AO}+ku_{BO}e^{j\frac{2\pi}{3}}+ku_{CO}e^{j\frac{4\pi}{3}}\\ &= \frac{ku_{\rm dc}}{2}\left(S_A+S_Be^{j\frac{2\pi}{3}}+S_Ce^{j\frac{4\pi}{3}}\right)\\ &= \frac{u_{\rm dc}}{3}\left(S_A+S_Be^{j\frac{2\pi}{3}}+S_Ce^{j\frac{4\pi}{3}}\right)\end{aligned} \tag{1}$$

where k equals 2/3 for equal-amplitude transformation. S_A, S_B, and S_C belong to the collection {-1, 0, 1}, representing state

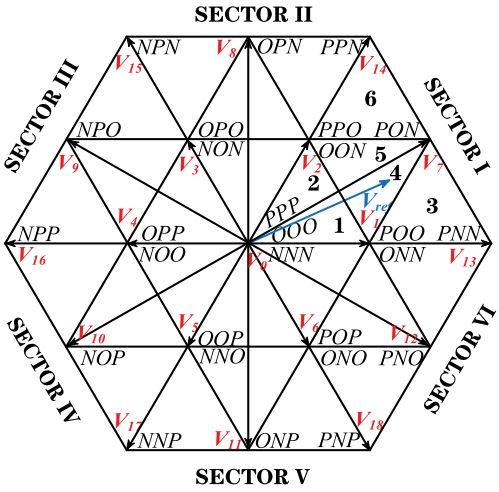

Fig. 2. Voltage vector distribution of three-level T-type inverter.

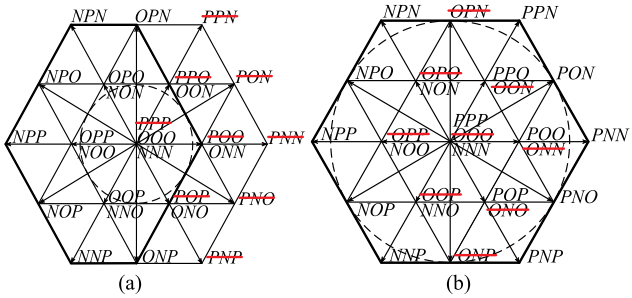

Fig. 3. Failed voltage vectors under single-switch open-circuit fault. (a) Open-circuit fault of S_{A1}. (b) Open-circuit fault of S_{A3}.

[N], [O], and [P]. The distribution of output voltage vector of 3LT^{2}I is shown as Fig. 2. In this article, seven-step space vector pulsewidth modulation (SVPWM) is applied and the reference voltage vector could be composed by three nearest vectors [28].

III. Single-Switch Open-Circuit Fault of Three-Level T-Type Inverter

A specific voltage vector cannot be composed if all the switch states for the vector fail. Whether the inverter is able to keep working in fault conditions can be judged by the remaining healthy voltage vectors. Open-circuit fault of switches can be divided into single-switch fault and multiple-switch fault and the former is studied in this article. The current path changes as a switch fails in 3LT^{2}I, which leads to abnormal output potential of the failed bridge.

A. Single-Switch Open-Circuit Fault

3LT^{2}I has two types of single-switch open-circuit faults: horizontal switch fault including S_{A2}, S_{A3}, S_{B2}, S_{B3}, S_{C2}, and S_{C3} open-circuit fault and vertical switch fault including S_{A1}, S_{A4}, S_{B1}, S_{B4}, S_{C1}, and S_{C4} open-circuit fault. For instance, five voltage vectors cannot be composed by the 3LT^{2}I when S_{A1} fails, as shown in Fig. 3(a). Modulation index should be limited because the area of valid vectors reduces. The maximum trajectory of reference voltage vector is shown in Fig. 3(a). As

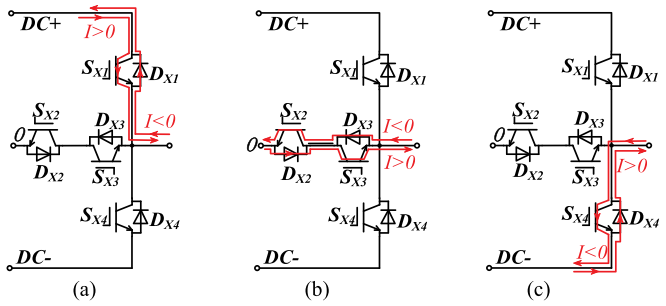

Fig. 4. Circuit path under normal condition. (a) Circuit path in state [P]. (b) Circuit path in state [O]. (c) Circuit path in state [N]. (X is A or B or C).

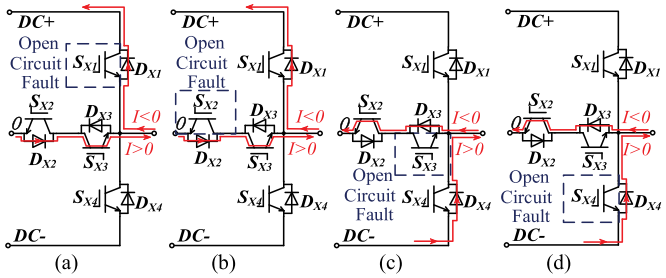

Fig. 5. Circuit path under single-switch open-circuit fault. (a) Circuit path in state [P] as S_{X1} fails. (b) Circuit path in state [O] as S_{X2} fails. (c) Circuit path in state [O] as S_{X3} fails. (d) Circuit path in state [N] as S_{X4} fails. (X is A or B or C).

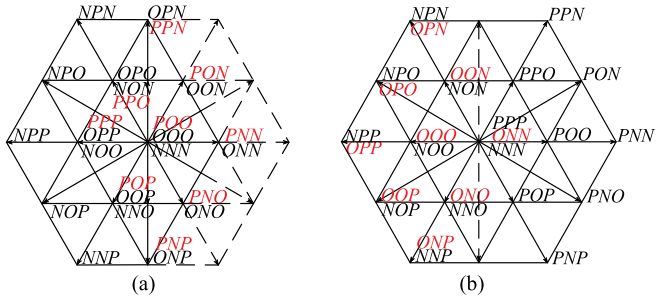

Fig. 6. Distortion of voltage vectors under single-switch open-circuit fault. (a) Open-circuit fault of S_{A1}. (b) Open-circuit fault of S_{A3}.

for horizontal switch S_{A3} fault, the area of valid voltage vectors remains the same, so there is no additional limitation of modulation index, as shown in Fig. 3(b). As the valid voltage vectors area is bigger than the inner hexagon, 3LT^{2}I is all able to keep running with fault-tolerant control method under 12 different single-switch open-circuit fault conditions. When fault-tolerant control method applied, failed medium vector such as "PON" can be equivalently replaced by two long vectors "PPN" and "PNN." As for short vector and zero vector, algorithm of redundant switch state replacement is utilized in fault-tolerant operation [8]–[10].

B. Current Path Under Single-Switch Open-Circuit Fault

The current path of the 3LT^{2}I depends on the load current and switch state. The current paths under normal condition are shown in Fig. 4.

TABLE II
THEORETICAL CALCULATION OF IDEAL VOLTAGE VECTOR TRAJECTORY WHEN S_{A1} FAILS ($0.578 < m \leq 1$)

Sector	Interval θ [rad]	$\lvert V_{inv\alpha}(\theta)\rvert$ [V]	$\lvert V_{inv\beta}(\theta)\rvert$ [V]
V-5	$\left[\frac{3\pi}{2}, \frac{3\pi}{2}+\psi(m)\right)$	$\lvert V_{ref}\rvert\cos\theta - \frac{u_{dc}}{3}\times\left[\frac{1}{2} - m\sin\left(\frac{5\pi}{3}-\theta\right)\right]$	$\lvert V_{ref}\rvert\sin\theta$
V-6	$\left[\frac{3\pi}{2}+\psi(m), \frac{5\pi}{3}\right)$	$\lvert V_{ref}\rvert\cos\theta - \frac{u_{dc}}{3}\times m\times\left[2\sin\left(\theta-\frac{4\pi}{3}\right)+\sin\theta\right]$	$\lvert V_{ref}\rvert\sin\theta$
VI-3	$\left[\frac{5\pi}{3}, \frac{11\pi}{6}-\psi(m)\right)$	$\lvert V_{ref}\rvert\cos\theta - \frac{u_{dc}}{3}\times m\sin\left(\theta-\frac{4\pi}{3}\right)$	$\lvert V_{ref}\rvert\sin\theta$
VI-4	$\left[\frac{11\pi}{6}-\psi(m), \frac{11\pi}{6}\right)$	$\lvert V_{ref}\rvert\cos\theta - \frac{u_{dc}}{3}\times\left[\frac{1}{2} + m\sin\left(\theta-\frac{5\pi}{3}\right)\right]$	$\lvert V_{ref}\rvert\sin\theta$
VI-5	$\left[\frac{11\pi}{6}, \frac{11\pi}{6}+\psi(m)\right)$	$\lvert V_{ref}\rvert\cos\theta - \frac{u_{dc}}{3}\times\left[2m\sin\left(\theta-\frac{4\pi}{3}\right)+m\sin\theta-\frac{1}{2}\right]$	$\lvert V_{ref}\rvert\sin\theta$
VI-6	$\left[\frac{11\pi}{6}+\psi(m), \pi\right)$	$\lvert V_{ref}\rvert\cos\theta - \frac{u_{dc}}{3}\times m\sin\left(\theta-\frac{4\pi}{3}\right)$	$\lvert V_{ref}\rvert\sin\theta$
I-3	$\left[\pi, \frac{\pi}{6}-\psi(m)\right)$	$\lvert V_{ref}\rvert\cos\theta - \frac{u_{dc}}{3}\times m\sin\left(\theta+\frac{\pi}{3}\right)$	$\lvert V_{ref}\rvert\sin\theta$
I-4	$\left[\frac{\pi}{6}-\psi(m), \frac{\pi}{6}\right)$	$\lvert V_{ref}\rvert\cos\theta - \frac{u_{dc}}{3}\times\left[2m\sin\left(\theta+\frac{\pi}{3}\right)-m\sin\theta-\frac{1}{2}\right]$	$\lvert V_{ref}\rvert\sin\theta$
I-5	$\left[\frac{\pi}{6}, \frac{\pi}{6}+\psi(m)\right)$	$\lvert V_{ref}\rvert\cos\theta - \frac{u_{dc}}{3}\times\left[\frac{1}{2} + m\sin\left(\frac{\pi}{3}-\theta\right)\right]$	$\lvert V_{ref}\rvert\sin\theta$
I-6	$\left[\frac{\pi}{6}+\psi(m), \frac{\pi}{3}\right)$	$\lvert V_{ref}\rvert\cos\theta - \frac{u_{dc}}{3}\times m\sin\left(\theta+\frac{\pi}{3}\right)$	$\lvert V_{ref}\rvert\sin\theta$
II-3	$\left[\frac{\pi}{3}, \frac{\pi}{2}-\psi(m)\right)$	$\lvert V_{ref}\rvert\cos\theta - \frac{u_{dc}}{3}\times m\times\left[2\sin\left(\frac{2\pi}{3}-\theta\right)-\sin\theta\right]$	$\lvert V_{ref}\rvert\sin\theta$
II-4	$\left[\frac{\pi}{2}-\psi(m), \frac{\pi}{2}\right)$	$\lvert V_{ref}\rvert\cos\theta - \frac{u_{dc}}{3}\times\left[\frac{1}{2} - m\sin\left(\theta-\frac{\pi}{3}\right)\right]$	$\lvert V_{ref}\rvert\sin\theta$

As switch S_{A1} fails, the current flows through the diode D_{A1} normally when the load current is reversed. But the current cannot flow through the failed switch S_{A1} and flows through D_{A2} and S_{A3} instead when the load current is forward as Fig. 5(a). The output potential of bridge A changes to neutral-point potential as well. It consequently leads to the distortion of the equivalent output voltage vector trajectory. During the abnormal operation period, the neutral-point potential u_O changes. It could be analyzed that the neutral-point potential increases as S_{A1} or S_{A2} fails and decreases as S_{A3} or S_{A4} fails.

IV. NOVEL SINGLE-SWITCH OPEN-CIRCUIT FAULT DIAGNOSIS METHOD BASED ON AVERAGE VOLTAGE VECTOR

The abnormal output potentials caused by single-switch open-circuit fault will result in output voltage vector distortion, which is the basis of the proposed diagnosis method.

A. Output Voltage Vector Distortion Under Single-Switch Open-Circuit Fault

Based on the current path variation regular for single-switch open-circuit fault, the output voltage vector distortion could be analyzed. When S_{A1} fails with load current i_A being forward and bridge A being of state [P], the current flows through D_{A2} and S_{A3}, and the output potential of bridge A is equal to the neutral-point potential. The distortion of output voltage vector can be predicted in Fig. 6(a). When S_{A3} fails with the load current i_A being forward and bridge A being of state [O], the current flows through D_{A4} and the output potential of bridge A is equal to the low side bus potential. The output voltage vector distortion under S_{A3} open-circuit fault is shown in Fig. 6(b).

B. Equivalent Voltage Vector Trajectory Distortion Under SVPWM Method

When the inverter is healthy, α-axis component $\boldsymbol{V}_{ref\alpha}$ and β-axis component $\boldsymbol{V}_{ref\beta}$ of $\boldsymbol{V}_{ref}$ can be obtained as follows:

$$\begin{cases} |\boldsymbol{V}_{ref\alpha}| = |\boldsymbol{V}_{ref}|\cos\theta \\ |\boldsymbol{V}_{ref\beta}| = |\boldsymbol{V}_{ref}|\sin\theta \end{cases} \tag{2}$$

where θ is the angle of reference voltage vector $\boldsymbol{V}_{\mathbf{ref}}$. The equivalent voltage vector $\boldsymbol{V}_{\mathbf{inv}}$ under open-circuit fault equals to the sum of reference voltage vector $\boldsymbol{V}_{\mathbf{ref}}$ and deviation voltage

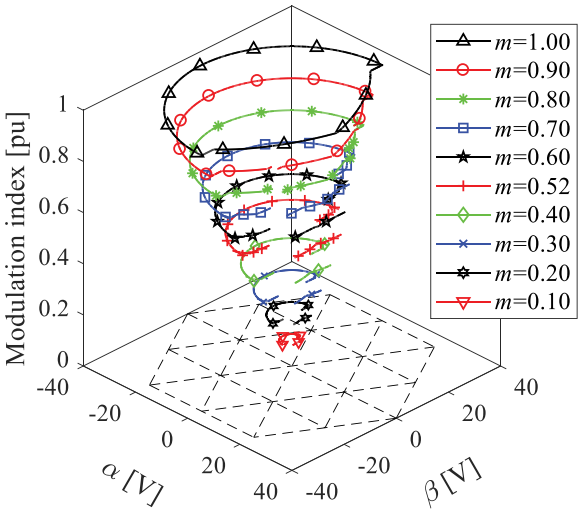

Fig. 7. Prediction of voltage vector trajectories under different m (S_{A1} fails).

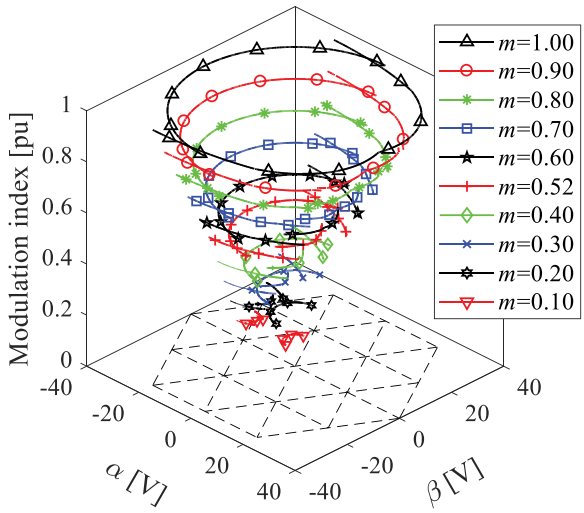

Fig. 8. Prediction of voltage vector trajectories under different m (S_{A3} fails).

vector $\Sigma\Delta\boldsymbol{V}_k \cdot \eta_k$ as follows:

$$\boldsymbol{V}_{\text{inv}} = \boldsymbol{V}_{\text{ref}} + \sum_{i=1}^{7} \Delta\boldsymbol{V}_k \cdot \eta_k \tag{3}$$

where $\Delta\boldsymbol{V}_k$ is the vector distortion of each switching state in a single switching cycle, and η_k is the proportion of each switching state in the switching cycle. $\boldsymbol{V}_{\mathbf{inv}}$'s component in α-axis direction and β-axis direction can be obtained as follows:

$$\begin{cases} |\boldsymbol{V}_{\text{inv}\alpha}| = |\boldsymbol{V}_{\text{ref}}| \cos\theta + \left|\sum_{i=1}^{7} \Delta\boldsymbol{V}_k \cdot \eta_k\right| \cos\varphi \\ |\boldsymbol{V}_{\text{inv}\beta}| = |\boldsymbol{V}_{\text{ref}}| \sin\theta + \left|\sum_{i=1}^{7} \Delta\boldsymbol{V}_k \cdot \eta_k\right| \sin\varphi \end{cases} \tag{4}$$

where φ is the angle of vector $\Sigma\Delta\boldsymbol{V}_k \cdot \eta_k$. The output equivalent voltage vector trajectory under single-switch open-circuit fault can be obtained by (4) as seven-step SVPWM is applied. Partial calculations are listed in Table II, where the interval depends on modulation index m. A function $\psi(m)$ is defined to simplify the formula as follows:

$$\psi(m) = \begin{cases} \frac{\pi}{2} - \arcsin\left(\frac{1}{2m}\right), \frac{1}{2} < m \le \frac{1}{\sqrt{3}} \\ \arcsin\left(\frac{1}{2m}\right) - \frac{\pi}{6}, \frac{1}{\sqrt{3}} < m \le 1 \end{cases} \tag{5}$$

Finally, the distorted trajectories of equivalent voltage vector under single-switch open-circuit fault under different value of modulation index can be predicted as Figs. 7 and 8.

C. Novel Diagnosis Method VVM Based on Average Voltage Vector

Based on the calculation abovementioned, twelve trajectories of single-switch open-circuit faults can be drawn as in Table III. Twelve trajectories have two types of irregular shape with six types of orientation, which provides two characteristics for identifying fault. Besides, deviation of the neutral-point potential Δu_O is also used to assist diagnosis especially when the shape characteristic is similar between vertical switch fault and horizontal switch fault. 3LT^{2}I average voltage vector in a fundamental cycle is near zero under healthy conditions. However, it becomes a stable vector with specific modulus and angle under single-switch open-circuit fault conditions. The modulus and angle information of it reflects the shape and orientation characteristics of each trajectories; therefore, average voltage vector is considered as the eigenvector in the process of diagnosis in the proposed VVM.

TABLE III
VOLTAGE VECTOR TRAJECTORIES AND EIGENVALUES UNDER SINGLE-SWITCH OPEN-CIRCUIT FAULT ($m = 0.8$)

Fault switch	Vector trajectory	α^*[rad]	Δu_O	Fault switch	Vector trajectory	α^*[rad]	Δu_O
S_{A1}		π	<0	S_{A3}		π	>0
S_{B1}		$5\pi/3$	<0	S_{B3}		$5\pi/3$	>0
S_{C1}		$\pi/3$	<0	S_{C3}		$\pi/3$	>0
S_{A4}		0	>0	S_{A2}		0	<0
S_{B4}		$2\pi/3$	>0	S_{B2}		$2\pi/3$	<0
S_{C4}		$4\pi/3$	>0	S_{C2}		$4\pi/3$	<0

Average voltage vector $\overline{\boldsymbol{V}_{\text{inv}}}$ in a fundamental cycle can be calculated as follows:

$$\begin{aligned} \overline{\boldsymbol{V}_{\text{inv}}} &= \frac{1}{T}\int_0^T \boldsymbol{V}_{\text{inv}}(t)dt \\ &= \frac{1}{T}\int_0^T [\boldsymbol{V}_{\text{inv}\alpha}(t) + \boldsymbol{V}_{\text{inv}\beta}(t)]dt \\ &= \overline{\boldsymbol{V}_{\text{inv}\alpha}} + \overline{\boldsymbol{V}_{\text{inv}\beta}} \end{aligned} \tag{6}$$

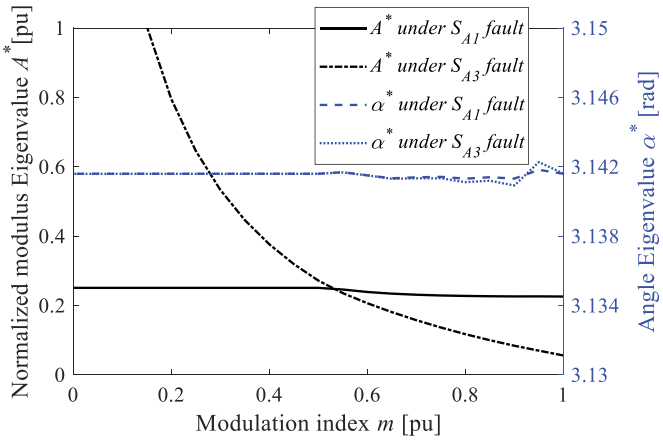

Fig. 9. Eigenvalues A^*&α^* of diagnosis variables A_{NORM}&α under different modulation indices (resistive load).

which is the eigenvector of proposed VVM.

Modulus of eigenvector is as follows:

$$\left|\overline{\boldsymbol{V}_{\mathrm{inv}}}\right| = \sqrt{\left|\overline{\boldsymbol{V}_{\mathrm{inv}\alpha}}\right|^2 + \left|\overline{\boldsymbol{V}_{\mathrm{inv}\beta}}\right|^2} \tag{7}$$

For convenience of comparison and analysis, $|\overline{\boldsymbol{V}_{\mathrm{inv}}}|$ is normalized to A_{NORM} as follows:

$$A_{\mathrm{NORM}} = \frac{\left|\overline{\boldsymbol{V}_{\mathrm{inv}}}\right|}{\left|\overline{\boldsymbol{V}_{\mathrm{ref}}}\right|} = \frac{\sqrt{\left|\overline{\boldsymbol{V}_{\mathrm{inv}\alpha}}\right|^2 + \left|\overline{\boldsymbol{V}_{\mathrm{inv}\beta}}\right|^2}}{mu_{dc}/\sqrt{3}} \tag{8}$$

which is the first diagnosis variable of the proposed VVM.

Angle of eigenvector is named α as follows:

$$\alpha = \angle\overline{\boldsymbol{V}_{\mathrm{inv}}} = \begin{cases} \arctan\dfrac{\left|\overline{\boldsymbol{V}_{\mathrm{inv}\alpha}}\right|}{\left|\overline{\boldsymbol{V}_{\mathrm{inv}\beta}}\right|}, \mathrm{Re}\left(\boldsymbol{V}_{\mathrm{inv}}\right) \geq 0 \\ \pi + \arctan\dfrac{\left|\overline{\boldsymbol{V}_{\mathrm{inv}\alpha}}\right|}{\left|\overline{\boldsymbol{V}_{\mathrm{inv}\beta}}\right|}, \mathrm{Re}\left(\boldsymbol{V}_{\mathrm{inv}}\right) < 0 \end{cases} \tag{9}$$

which is the second diagnosis variable of the proposed VVM.

Deviation of neutral-point potential Δu_O, the third diagnosis variable, can be calculated by voltage of $\mathrm{C_{high}}$ and $\mathrm{C_{low}}$ as follows:

$$\Delta u_O = \frac{1}{2} \times \left(u_{\mathrm{low}} - u_{\mathrm{high}}\right) \tag{10}$$

where u_{low} and u_{high} are the voltage of capacitor $\mathrm{C_{low}}$ and $\mathrm{C_{high}}$, respectively. Two dc-link capacitors' voltages will increase or decrease under fault conditions because the neutral-point current could not be balanced. The relationship between Δu_O and failed switch are summarized as Table III according to the current path variation analysis abovementioned.

Diagnosis variable A_{NORM} and α will have some certain values under single-switch open-circuit fault conditions. The particular values corresponding to 12 switch faults are defined as eigenvalue A^* and α^*, which can be calculated by (8) and (9) as Table III and Fig. 9. The eigenvalue A^* is the key parameter of threshold *TH* calculation for diagnosis variable A_{NORM} in VVM.

The flowchart of the proposed VVM is shown as Fig. 10. Eigenvalue A^* and α^* is calculated by modulation index *m* in the procedure "trajectory prediction" and the threshold *TH* needs to

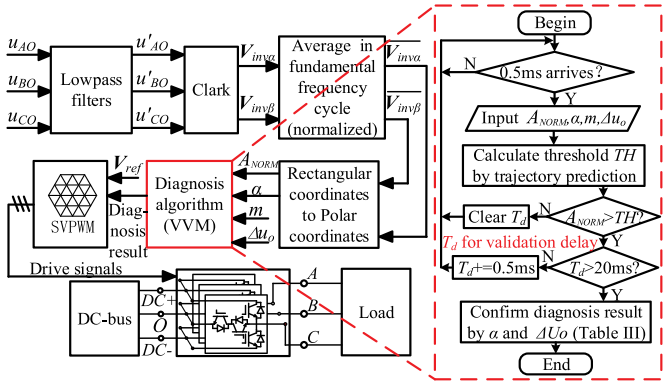

Fig. 10. Flowchart of the proposed VVM.

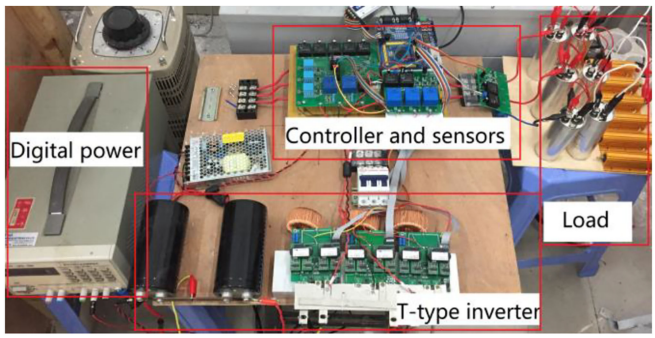

Fig. 11. Experiment platform of three-level T-type inverter.

be big enough to avoid misdiagnosis. Also, threshold *TH* needs to be smaller than the eigenvalue A^* to confirm fault conditions. Once a switch fails, diagnosis variable A_{NORM} exceeds *TH* and the fault conditions could be confirmed after a short delay. Then, fault switch could be identified by α and Δu_O. Twelve different single switch faults correspond to twelve kinds of eigenvalue combinations. The flow chart of CVM in this article is basically the same as that of VVM. There are two implementation differences between them including main sampled physical quantities and threshold calculation algorithm.

V. Simulation and Experiment

To verify the proposed VVM for single-switch open-circuit fault diagnosis, $3LT^2I$ systems were built on simulation platform and experiment platform as Figs. 1 and 11, the parameters of which are listed in Table IV.

The load resistance needs to be adjusted to change the power factor of load. Load impedance $\boldsymbol{Z}$ could be calculated by inductance *L*, capacitance *C*, and resistance *R* as follows:

$$\boldsymbol{Z}\left(j\omega\right) = j\omega L + \frac{R/j\omega C}{R + 1/j\omega C} \tag{11}$$

Simulations and experiments based on proposed VVM were carried out for two aspects of validation including method's performance under different PFs and performance under different modulation indices. Open-circuit fault of switches was emulated by shielding driving signals. Modulation index equals 0.8 and load resistance *R* is adjusted to get different pPFs as Table V. Diagnosis variables in VVM and CVM are both presented in

TABLE IV
PARAMETERS OF 3LT^{2}I SYSTEM IN SIMULATION AND EXPERIMENT

Parameters	Symbols	Value
Input dc-link voltage	u_{dc}	60V
Dc-link capacitor	C_{high}, C_{low}	4700μF
Switching frequency	f_S	10kHz
Rated frequency	f_R	50Hz
Load inductance	L_A, L_B, L_C	25mH
Load capacitance	C_A, C_B, C_C	200μF

TABLE V
PARAMETERS OF LOAD

Resistance[Ω]	Impedance $\boldsymbol{Z}$ [Ω]	Power factor [pu]
8	$7.90\angle 36.0°$	0.809(lag)
16	$7.95\angle$-1.1°	0.999(lead)
32	$8.01\angle$-37.8°	0.790(lead)

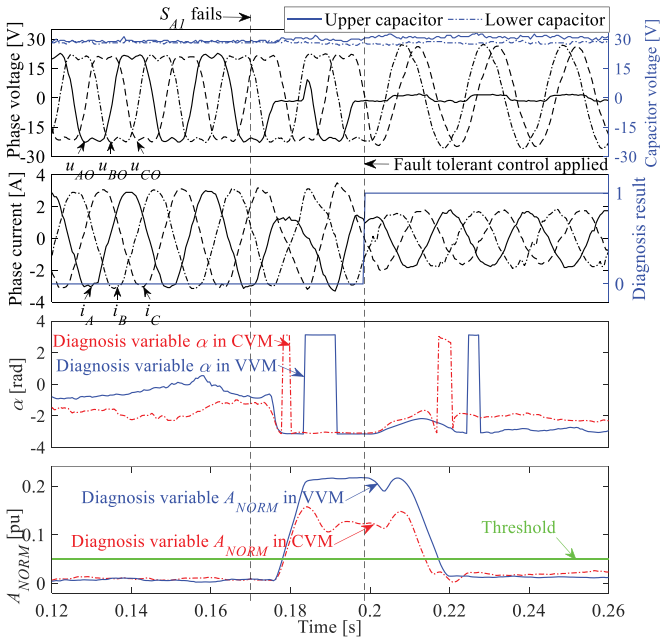

Fig. 13. Experiment of fault-tolerant control when S_{A1} fails ($m = 0.8$, $R = 16\ \Omega$).

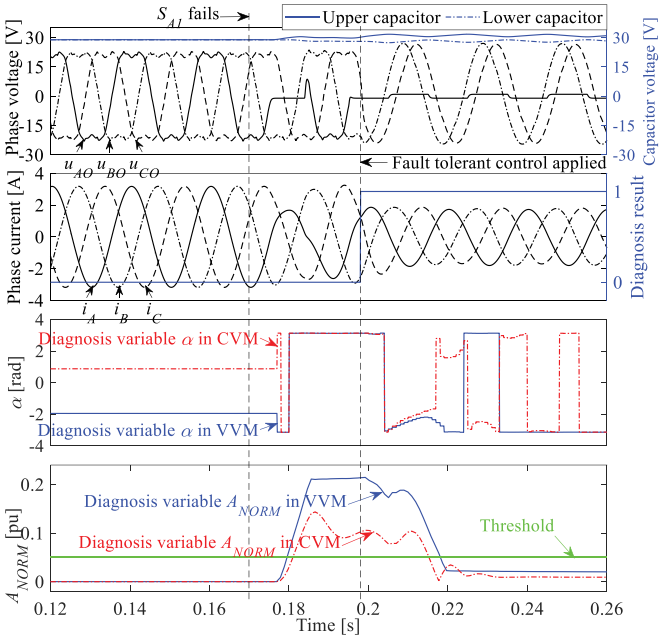

Fig. 12. Simulation of fault-tolerant control when S_{A1} fails ($m = 0.8$, $R = 16\ \Omega$).

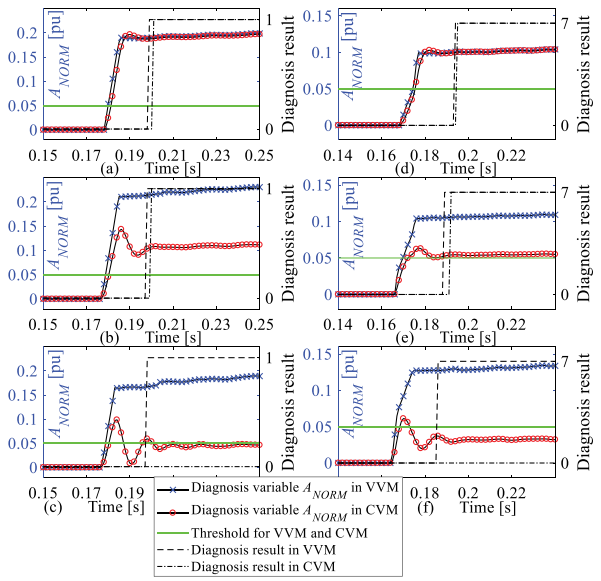

Fig. 14. Methods comparison simulation under different power factors ($m =$ 0.8pu and fault tolerant control is not applied). (a) $R = 8\ \Omega$ and S_{A1} fails at 0.17 s. (b) $R = 16\ \Omega$ and S_{A1} fails at 0.17 s. (c) $R = 32\ \Omega$ and S_{A1} fails at 0.17 s. (d) $R = 8\ \Omega$ and S_{A2} fails at 0.16s. (e) $R = 16\ \Omega$ and S_{A2} fails at 0.16s. (f) $R = 32\ \Omega$ and S_{A2} fails at 0.16 s.

figures for comparison because the proposed VVM is directly inherited from CVM. Normalization strategy was applied in two methods in simulations and experiments.

Figs. 12 and 13 show the diagnosis process of single-switch fault of S_{A1} by proposed VVM, where load resistance R equals 16 Ω. Before S_{A1} fails, voltages u_{AO}, u_{BO}, and u_{CO} are balanced so that the diagnosis variable A_{NORM} is near zero and diagnosis variable α is random due to the small disturbance. Variable α converges to eigenvalue α^* once the distortion begins, whereas A_{NORM} needs half a fundamental cycle to reach the eigenvalue A^*. The diagnosis result of conventional CVM is not utilized in the control process, but the diagnosis variables of it are presented as well. It can be seen in the results that the curve A_{NORM} in proposed VVM converges rapidly whereas curve A_{NORM} in conventional CVM converges to a lower eigenvalue A^* with oscillation.

Figs. 14 and 15 compare the curves of diagnosis variables A_{NORM} of two methods in simulations and experiments. Curves of variables α in two methods are not drawn here because they

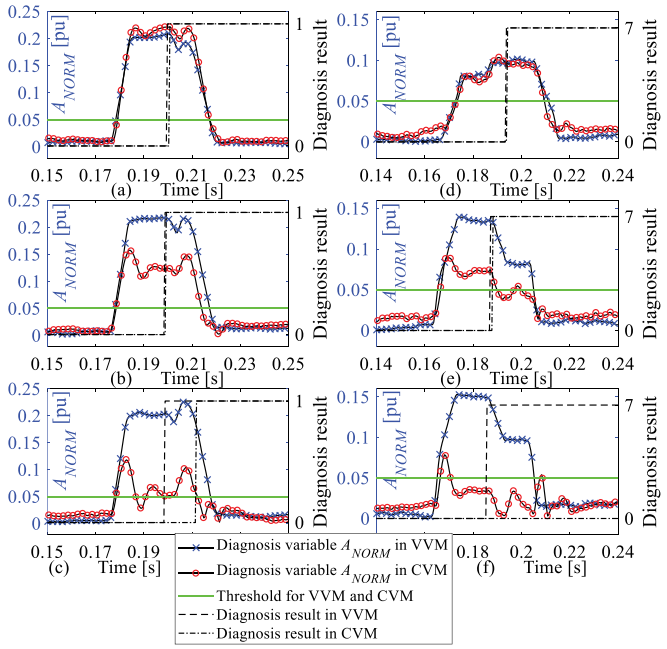

Fig. 15. Methods comparison experiment under different power factors ($m = 0.8$ pu). (a) $R = 8\ \Omega$ and S_{A1} fails at 0.17 s. (b) $R = 16\ \Omega$ and S_{A1} fails at 0.17 s. (c) R=32 Ω and S_{A1} fails at 0.17 s. (d) $R = 8\ \Omega$ and S_{A2} fails at 0.16 s. (e) $R = 16\ \Omega$ and S_{A2} fails at 0.16 s. (f) $R = 32\ \Omega$ and S_{A2} fails at 0.16 s.

are exactly the same under S_{A1} fault and S_{A2} fault, whose eigenvalues are perfectly consistent with that in Table III under different PFs. The diagnosis variable A_{NORM} in proposed VVM converges quickly after single-switch open circuit fault while A_{NORM} in CVM has high amplitude oscillation after switch fault. The CVM fails to detect the fault as the resistance increase to 32 Ω because the eigenvalue A^* reduces to a small value when the load becomes capacitive. It needs to be emphasized that the fault-tolerant control algorithm is not be applied in simulations of Fig. 14, which is for better comparison of two methods' performance.

Figs. 16 and 17 present the voltage vector trajectories under normal conditions, fault conditions, and conditions with fault tolerant control. The irregular trajectories under fault conditions depend on the power factor because the output voltage vector distortion not only depends on the fault switch, but also is related to the current direction. Taking S_{A1} fault for example, if the load currents are capacitive, the fault phase current reduces to zero in advance and the current flows toward neutral-point during state [P], which performs normally for the inverter and makes the voltage vector trajectory turn to the normal circle in advance as Fig. 16(c). It needs to be emphasized that the sampling point is uniformly distributed in time but not in trajectory length under fault conditions, and the direction of trajectory's deviation at each sampling instant are highly consistent. Hence, eigenvalues α^* could be independent from load power factor.

Additionally, contrast simulations and experiments were carried out in three modulation index 0.4, 0.6, and 0.8 with load resistance R setting 16 Ω.

Figs. 18 and 19 show the voltage vector trajectory in simulation and experiment, where the distorted trajectory shape varies

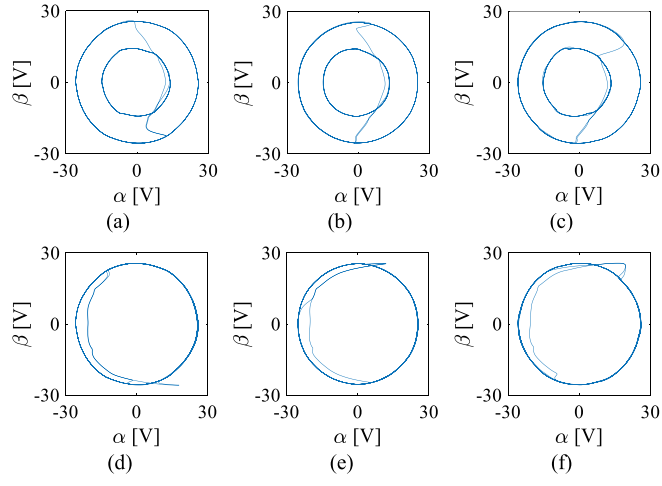

Fig. 16. Voltage vector trajectories in simulation under single-switch open-circuit fault under different power factors of load ($m = 0.8$ pu). (a) S_{A1} fails and $R = 8\ \Omega$. (b) S_{A1} fails and $R = 16\ \Omega$. (c) S_{A1} fails and $R = 32\ \Omega$. (d) S_{A2} fails and $R = 8\ \Omega$. (e) S_{A2} fails and $R = 16\ \Omega$. (f) S_{A2} fails and $R = 32\ \Omega$.

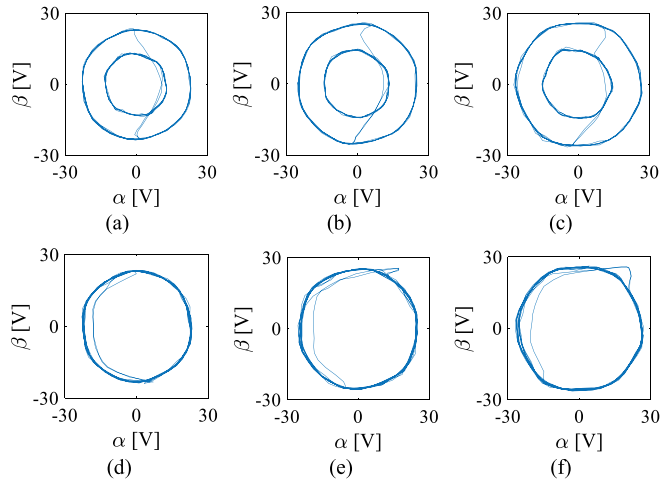

Fig. 17. Voltage vector trajectories in experiment under single-switch open-circuit fault under different power factors of load ($m = 0.8$ pu). (a) S_{A1} fails and $R = 8\ \Omega$. (b) S_{A1} fails and $R = 16\ \Omega$. (c) S_{A1} fails and $R = 32\ \Omega$. (d) S_{A2} fails and $R = 8\ \Omega$. (e) S_{A2} fails and $R = 16\ \Omega$. (f) S_{A2} fails and $R = 32\ \Omega$.

with modulation index. When vertical switch fails with m bigger than 0.5, the trajectory becomes a smaller circle when fault tolerant control applied. The distorted trajectories are basically consistent with that in trajectory prediction. Shapes of distorted trajectories under different modulation indices are similar to each other under S_{A1} fault condition and has bigger distinction under S_{A2} fault condition. The current vector trajectories in simulation are also depicted as Fig. 20 for comparison, it can be seen that the distorted trajectories are less sensitive for diagnosis in the aspect of average vector calculation.

In Table VI, the performance indices of two methods under different PFs are listed for quantitative analysis. In proposed VVM, the adjusting time is within 0.01 s and overshoot does not exist after switch fault. Besides, eigenvalue A^* increases from 0.101 to 0.128 pu as load resistance R increases from 8 to 32 Ω under S_{A1} fault condition whereas A^* has a biggest value 0.214 pu under S_{A2} fault condition. As for CVM, the

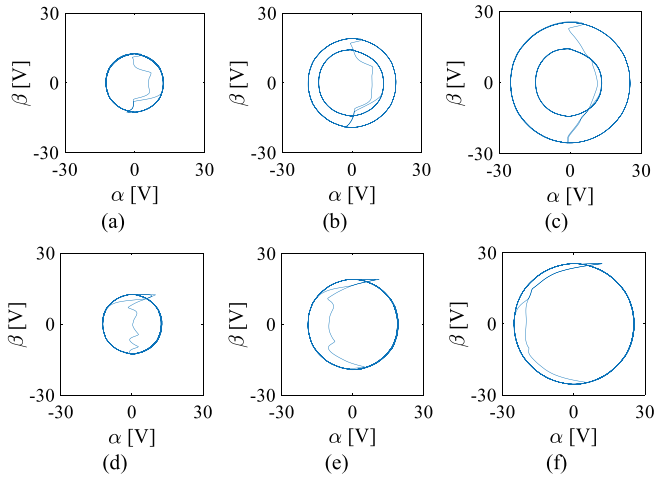

Fig. 18. Voltage vector trajectories in simulation under single-switch open-circuit fault under different modulation indices ($R = 16\ \Omega$). (a) S_{A1} fails and $m = 0.4$ pu. (b) S_{A1} fails and $m = 0.6$ pu. (c) S_{A1} fails and $m = 0.8$ pu. (d) S_{A2} fails and $m = 0.4$ pu. (e) S_{A2} fails and $m = 0.6$ pu. (f) S_{A2} fails and $m = 0.8$ pu.

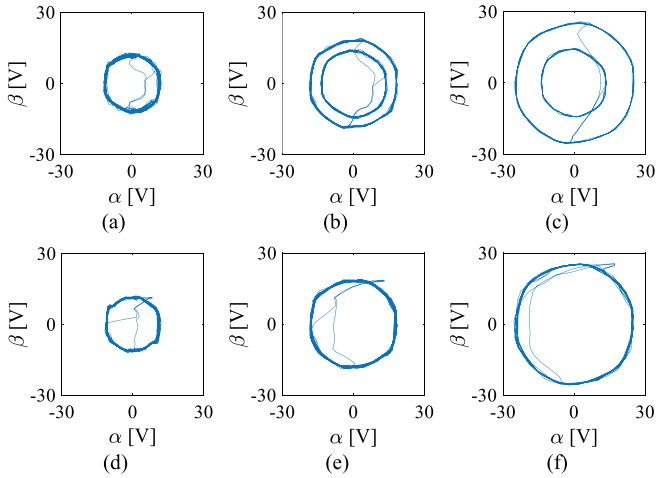

Fig. 19. Voltage vector trajectories in experiment under single-switch open-circuit fault under different modulation indices ($R = 16\ \Omega$). (a) S_{A1} fails and $m = 0.4$ pu, (b) S_{A1} fails and $m = 0.6$ pu. (c) S_{A1} fails and $m = 0.8$ pu. (d) S_{A2} fails and $m = 0.4$ pu. (e) S_{A2} fails and $m = 0.6$ pu. (f) S_{A2} fails and $m = 0.8$ pu.

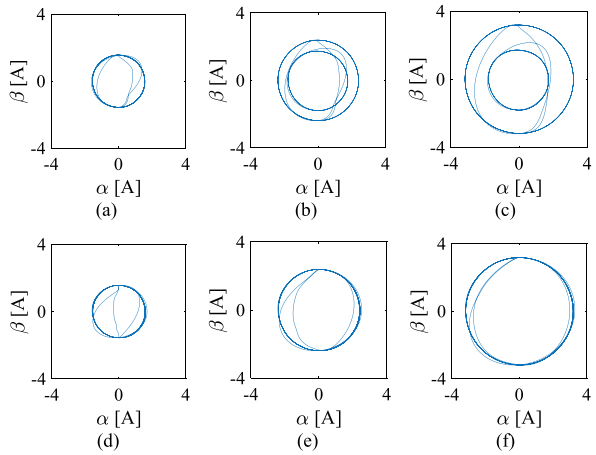

Fig. 20. Current vector trajectories in simulation under single-switch open-circuit fault under different modulation indices ($R = 16\ \Omega$). (a) S_{A1} fails and $m = 0.4$ pu. (b) S_{A1} fails and $m = 0.6$ pu. (c) S_{A1} fails and $m = 0.8$ pu. (d) S_{A2} fails and $m = 0.4$ pu. (e) S_{A2} fails and $m = 0.6$ pu. (f) S_{A2} fails and $m = 0.8$ pu.

TABLE VI
COMPARISON OF TWO METHODS' PERFORMANCE ($m = 0.8$)

Diagnosis method	R [Ω]	Failed switch	Adjusting time [s]	Overshoot [%]	A^* [pu]
Proposed VVM	8	S_{A1}	0.008	0	0.190
		S_{A2}	0.009	0	0.101
	16	S_{A1}	0.010	0	0.214
		S_{A2}	0.010	0	0.105
	32	S_{A1}	0.007	0	0.166
		S_{A2}	0.010	0	0.128
Conventional CVM	8	S_{A1}	0.009	3.6	0.190
		S_{A2}	0.010	2.9	0.100
	16	S_{A1}	0.020	35.6	0.106
		S_{A2}	0.016	17.7	0.054
	32	S_{A1}	0.046	131.7	0.044
		S_{A2}	0.030	99.0	0.032

adjusting time is close to half a fundamental cycle 0.01 s when R is 8 Ω but increases to several fundamental cycles with higher R. Eigenvalue A^* in CVM with 8 Ω load resistance basically equal to the ones in VVM, but decrease dramatically as the load resistance R added. Overshoots in CVM are obvious.

The relationship between methods' performance and PFs can be summarized combining with the trajectory analysis in Figs. 16 to 20. The eigenvalue A^* in proposed VVM only depends on the abnormal duration of the distortion because the normal part of distorted trajectory overlaps with the original circle. Consequently, the floating of eigenvalue A^* in VVM under different PFs under switch fault is limited. In another aspect, the adjusting time of A_{NORM} is within half a fundamental cycle because the distorted trajectories are fixed once the load and modulation index are settled. As for conventional CVM, the current curves are more likely to be symmetric when the load is capacitive, leading to the oscillation and deviation of the current vector trajectory in normal half cycle under fault conditions. On the one hand, the current vector trajectory is narrowed and the modulus eigenvalue A^* gets smaller, which means that smaller threshold value should be set in diagnosis. The smaller threshold in CVM eventually reduces the robustness for load regulation. On the other hand, diagnosis variable A_{NORM} needs more time to be stable than that in VVM when switch fails after a switch fault.

Finally, simulations of proposed VVM and conventional CVM under different modulation indices and different PFs were carried out for further analysis. The eigenvalues A^* under different conditions are depicted as Fig. 21. The eigenvalues of two methods basically remain the same under different values of m as

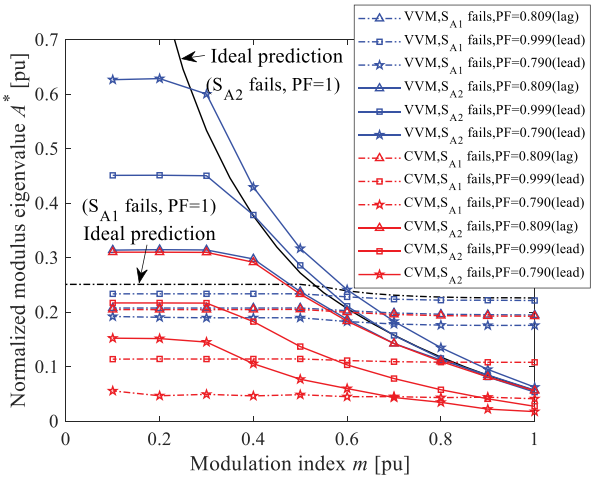

Fig. 21. Variation of normalized modulus eigenvalue in VVM and CVM under different modulation indices and different power factors.

S_{A1} fails. However, the eigenvalue decreases with the reduction of m under S_{A2} fault condition. The eigenvalues approach a constant value as m approaches zero, which is different from the prediction because the current cannot keep being negative for long time when m is small. Comparing the eigenvalue curves in CVM and VVM with the ideal predicted curves, we could find that the eigenvalue A^* in two methods is big enough for threshold setting under small modulation index. But, the eigenvalue A^* in CVM reduces to 0.017 pu under S_{A2} fault condition with the PF equaling 0.790 pu (lead) and the modulation index m equaling 1 pu. The CVM becomes extremely sensitive as it needs a threshold smaller than 0.017 pu, whereas VVM is able to set a higher threshold because the eigenvalues A^* is much higher.

It can be concluded by the performance analysis of two methods that the proposed VVM needs a confirming delay at around one fundamental cycle. Higher thresholds can be set under different PFs and different modulation indices, which is significant for 3LT^{2}I to eliminate load regulation disturbance. The proposed VVM not only inherits the advantages of high diagnostic accuracy from CVM, but also alleviates the contradiction between small eigenvalues of diagnosis variable and a high thresholds requirement.

VI. Conclusion

This article proposes a new method (VVM) for single-switch open-circuit fault diagnosis in 3LT^{2}I based on average voltage vector and neutral-point potential. Dc-link neutral-point to bridge output terminal voltages utilized in diagnosis inhibit the influence of load current under healthy condition and diagnosis variable oscillation under fault conditions, shrink the eigenvalue's variation range under different PFs, and enhance the reliability and robustness of diagnosis process. Trajectory prediction provides a theoretical basis for threshold setting, improves the suitability of diagnosis under different modulation indices, and provides a novel concept for fault diagnosis. The proposed approach is feasible for a large range of PFs in any modulation index. However, the procedure is sensitive to dc-bus voltage variation and modulus index regulation, which can be overcame by further trajectory prediction and compensation technique. The method is suitable for three-level and two-level inverters with passive load, but needs further research for other applications.

References

[1] M. Schweizer, I. Lizama, T. Friedli, and J. W. Kolar, "Comparison of the chip area usage of 2-level and 3-level voltage source converter topologies," in *Proc. 36th Annu. Conf. IEEE Ind. Electron. Soc.*, Glendale, AZ, USA, 2010, pp. 391–396.

[2] A. Nabae, I. Takahashi, and H. Akagi, "A New Neutral-Point-Clamped PWM Inverter," *IEEE Trans. Ind. Appl.*, vol. IA-17, no. 5, pp. 518–523, Sep. 1981.

[3] N. Celanovic and D. Boroyevich, "A comprehensive study of neutral-point voltage balancing problem in three-level neutral-point-clamped voltage source PWM inverters," *IEEE Trans. Power Electron.*, vol. 15, no. 2, pp. 242–249, Mar. 2000.

[4] H. Abu-Rub, J. Holtz, J. Rodriguez, and G. Baoming, "Medium-Voltage Multilevel Converters—State of the Art, Challenges, and Requirements in Industrial Applications," *IEEE Trans. Ind. Electron.*, vol. 57, no. 8, pp. 2581–2596, Aug. 2010.

[5] M. Schweizer and J. W. Kolar, "Design and implementation of a hybrid efficient three-level T-type converter for low-voltage applications," *IEEE Trans. Power Electron.*, vol. 28, no. 2, pp. 899–907, Feb. 2013.

[6] Y. Wang, W. W. Shi, N. Xie, and C. M. Wang, "Diode free T-type three level neutral-point-clamped inverter for low voltage renewable energy system," *IEEE Trans. Ind. Electron.*, vol. 61, no. 11, pp. 6168–6174, Nov. 2014.

[7] U. Choi, J. Lee, and K. Lee, "New modulation strategy to balance the neutral-point voltage for three-level neutral-clamped inverter systems," *IEEE Trans. Energy Convers.*, vol. 29, no. 1, pp. 91–100, Mar. 2014.

[8] U.-M. Choi, F. Blaabjerg, and K.-B. Lee, "Reliability improvement of a T-type three-level inverter with fault-tolerant control strategy," *IEEE Trans. Power Electron.*, vol. 30, no. 5, pp. 2660–2673, May 2015.

[9] J. Chen, C. Zhang, A. Chen, and X. Xing, "Fault-tolerant control strategies for t-type three-level inverters considering neutral-point voltage oscillations," *IEEE Trans. Ind. Electron.*, vol. 66, no. 4, pp. 2837–2846, Apr. 2019.

[10] X. Li, S. Dusmez, B. Akin and K. Rajashekara, "A new active fault-tolerant SVPWM strategy for single-phase faults in three-phase multilevel converters," *IEEE Trans. Ind. Electron.*, vol. 62, no. 6, pp. 3955–3965, Jun. 2015.

[11] S. Karimi, A. Gaillard, P. Poure, and S. Saadate, "FPGA-based real-time power converter failure diagnosis for wind energy conversion system," *IEEE Trans. Ind. Electron.*, vol. 55, no. 12, pp. 4299–4308, Dec. 2008.

[12] Z. Li, H. Ma, Z. Bai, Y. Wang, and B. Wang, ''Fast transistor open-circuit faults diagnosis in grid-tied three-phase VSIs based on average bridge arm pole-to-pole voltages and error-adaptive thresholds," *IEEE Trans. Power Electron.*, vol. 33, no. 9, pp. 8040–8051, Sep. 2018.

[13] B. Lu and S. Sharma, "A literature review of IGBT fault diagnostic and protection methods for power inverters," *IEEE Trans. Ind. Appl.*, vol. 45, no. 5, pp. 1770–1777, Sep./Oct. 2009.

[14] S. A. E. Moussa, M. Jean-Philippe, and P. Serge, "Zero-sequence current based diagnostic method for open-switch fault detection in parallel inverters system," *IEEE Trans. Power Electron.*, vol. 34, no. 4, pp. 3750–3764, Apr. 2019.

[15] M. S. Shadlu, "Fault detection and diagnosis in voltage source inverters using principle component analysis," in *Proc. IEEE 4th Int. Conf. Knowl. Based Eng. Innov.*, Tehran, Iran, 2017, pp. 509–515.

[16] Y. Mei and H. Yuan, "A novel open-circuit fault diagnosis method for voltage source inverter," in *Proc. Power Energy Autom.*, Shenzhen, China, 2018, pp. 1819–1824.

[17] W. Sleszynski, J. Nieznanski, and A. Cichowski, "Open-transistor fault diagnostics in voltage-source inverters by analyzing the load currents," *IEEE Trans. Ind. Electron.*, vol. 56, no. 11, pp. 4681–4688, Nov. 2009.

[18] U. Choi, K. Lee, and F. Blaabjerg, "Diagnosis and tolerant strategy of an open-switch fault for t-type three-level inverter systems," *IEEE Trans. Ind. Appl.*, vol. 50, no. 1, pp. 495–508, Jan./Feb. 2014.

[19] U. M. Choi, K. B. Lee, and F. Blaabjerg, "Diagnosis method of an openswitch fault for a grid-connected T-type three-level inverter system," in *Proc. 3rd IEEE Int. Symp. Power Electron. Distrib. Gener. Syst.*, Raleigh, NC, USA, 2012, pp. 470–475.

[20] A. Topcu and Y. Sozer, "Multiple Device Open-Circuit Fault Diagnosis for T-Type Multilevel Inverters," in *Proc. IEEE Energy Convers. Congr. Expo.*, Portland, OR, USA, 2018, pp. 4056–4061.
[21] J. He, N. A. O. Demerdash, N. Weise, and R. Katebi, "A fast online diagnostic method for open-circuit switch faults in SiC-MOSFET based T-type multilevel inverters," *IEEE Trans. Ind. Appl.*, vol. 53, no. 3, pp. 2948–2958, May 2017.
[22] Z. Li *et al.*, "Open-transistor faults diagnosis in voltage-source inverter based on phase voltages with sliding-window counting method," in *Proc. 42nd Annu. Conf. IEEE Ind. Electron. Soc.*, 2003, vol. 2, pp. 435–440.
[23] C. Shu, C. Ya-Ting, Y. Tian-Jian, and W. Xun, "A novel diagnostic technique for open-circuit faults of inverters based on output line-to-line voltage model," *IEEE Trans. Ind. Electron.*, vol. 63, no. 7, pp. 4412–4421, Jul. 2016.
[24] B. Cai, Y. Zhao, H. Liu, and M. Xie, "A data-driven fault diagnosis methodology in three-phase inverters for PMSM drive systems," *IEEE Trans. Power Electron.*, vol. 32, no. 7, pp. 5590–5600, Jul. 2017.
[25] M. A. Rodriguez-Blanco, A. Vazquez-Perez, L. Hernandez-Gonzalez, V. Golikov, J. Aguayo-Alquicira, and M. May-Alarcon, "Fault detection for IGBT using adaptive thresholds during the turn-on transient," *IEEE Trans. Ind. Electron.*, vol. 62, no. 3, pp. 1975–1983, Mar. 2014.
[26] B. Wang, P. T. Krein, H. Ma, Z. Bai, and Z. Li, "Fast diagnosis of multiple open-circuit faults in a t-type inverter based on voltages across half-bridge switches," in *Proc. Power Energy Autom. Conf.*, Shenzhen, China, 2018, pp. 1098–1103.
[27] J. He and N. A. O. Demerdasd, "Diagnosis of open-circuit switch faults in multilevel active-NPC (ANPC) inverters," in *Proc. Transp. Electrific. Conf. Expo.,* Dearborn, MI, USA, 2014, pp. 1–6.
[28] F. Chen and W. Qiao, "A general space vector PWM scheme for multilevel inverters," in *Proc. IEEE Energy Convers. Congr. Expo.*, Milwaukee, WI, USA, 2016, pp. 1–6.

Yiqing Liang was born in Zhejiang, China. He received the B.S. degree in electrical engineering from Huaqiao University, Xiamen, China, in 2019. He is currently working toward the Ph.D. degree with the Institute of Modern Physics, Chinese Academy of Sciences, Beijing China.

His current research interests mainly focus on multilevel converter, and fault tolerant operation strategy.

Rongkun Wang was born in Fujian, China. He received the Ph.D. degree in electrical engineering from the Institute of Modern Physics, Chinese Academy of Sciences, Beijing China, in 2013.

He is currently a Master Instructor in Huaqiao University, Quanzhou, China. His current research interests mainly focus on power electronics and power drives, devoting to digital UPS and its parallel technology, the control of the permanent magnet synchronous linear motor, harmonic detection method and three-level active filter, and other innovative research. He has been a major participant in the study of major national science and technology projects and the Chinese Academy of Sciences' directional projects.

Bingtao Hu was born in Anhui, China. He is currently working toward the master's degree with Huaqiao University, Quanzhou, China.

He has worked on the electric drive and power conversion technology.